The Astrophysical Journal Supplement Series, 154:160–165, 2004 September

24 MICRON PROPERTIES OF X-RAY–SELECTED ACTIVE GALACTIC NUCLEI

J. R. Rigby,[1] G. H. Rieke,[1] R. Maiolino,[2] R. Gilli,[2] C. Papovich,[1] P. G. Pérez-González,[1] A. Alonso-Herrero,[1] E. Le Floc'h,[1] C. W. Engelbracht,[1] K. Gordon,[1] D. C. Hines,[1,3] J. L. Hinz,[1] J. E. Morrison,[1] J. Muzerolle,[1] M. J. Rieke,[1] and K. Y. L. Su[1]

Received 2004 March 26; accepted 2004 May 21

ABSTRACT

We examine the 24 μm to X-ray color of 157 X-ray–selected active galactic nuclei (AGNs) as a function of X-ray obscuration and optical classification in the Chandra Deep Field–South. The sample consists of the *Chandra* hard-band detections with 2–8 keV flux above 10^{-15} ergs s^{-1} cm^{-2}. A deep 24 μm mosaic obtained with *Spitzer* provides mid-infrared fluxes for the sample. Since obscured AGNs locally have higher 24 μm/2–8 keV flux ratios than unobscured AGNs, and since X-ray background models predict a large population of obscured AGNs, we expect to find many X-ray–hard, IR-bright AGNs. Instead, we find that the 24 μm to X-ray flux ratio does not depend on X-ray hardness in the full sample, nor does it differ between narrow- and broad-line AGNs. We identify five nearly Compton-thick AGNs and find they have similar 24 μm to X-ray flux ratios compared to the full sample. We consider AGNs in the narrow redshift spikes at $z \sim 0.7$; for these AGNs, there is some evidence that the flux ratio increases with X-ray hardness. The redshift slice also shows an odd trend that is also prominent in the full sample: a group of X-ray–hard AGNs with very low 24 μm to X-ray flux ratios.

Subject headings: galaxies: active — infrared: galaxies — X-rays: galaxies

1. INTRODUCTION

The hard spectrum of the X-ray background, which peaks at 30–40 keV, implies the existence of a large population of obscured active galactic nuclei (AGNs; Madau et al. 1994; Comastri et al. 1995; Gilli et al. 2001). Finding and understanding these obscured AGNs is crucial to understanding the accretion history of the universe. These AGNs are predicted to be particularly bright in the mid-infrared, as soft X-ray and ultraviolet emission is absorbed by the intervening material and re-emitted by dust. With the *Infrared Space Observatory* (*ISO*), Fadda et al. (2002) reported elevated mid-infrared emission from obscured AGNs, and Franceschini et al. (2002) found the majority of *ISO*-detected AGNs to be obscured.

Spitzer can test these ideas about the obscuration of AGNs and the interplay of the infrared and X-ray backgrounds. By studying the Chandra Deep Field–South (CDF-S),[4] we are able to present a first look at the *Spitzer* mid-infrared properties of AGNs.

2. THE DATA AND CATALOGS

We present deep new observations of the CDF-S at 24 μm, obtained with the Multiband Imaging Photometer for *Spitzer* (MIPS; Rieke et al. 2004). These data were obtained with guaranteed time under Program ID 81 (*Spitzer* AORs 0008950528, 0008951296, 0008954112, 0008957696, 0008958208, 0008958464, 0008958976, 0008959488, 0008960000, 0008960512, 0008961024, and 0008961536). Slow scan-map mode was used, achieving an average integration of 1380 s. The data were reduced using the Data Analysis Tool (DAT) package of the MIPS instrument team (Gordon et al. 2004). The resulting mosaic completely overlaps the approximately $17' \times 17'$ *Chandra* field. The 80% completeness limit, determined by adding artificial sources, is 0.083 mJy (Papovich et al. 2004). This flux limit is comparable to the 5 σ noise, which, scaling from Dole et al. (2004), is 0.086 mJy at the CDF-S exposure depth (accounting for detector and confusion noise; Dole et al. 2004). Thus, the full mosaic is one of the deepest, widest field 24 μm maps yet obtained.

Sources were extracted from the 24 μm mosaic as described by Papovich et al. (2004). In the 270 arcmin^2 region having X-ray exposure times exceeding 0.5 Ms, we detect 1147 24 μm sources brighter than the 80% completeness limit. In the 200 arcmin^2 region having better than 0.75 Ms X-ray coverage, we detect 878 such 24 μm sources. (The X-ray depth of coverage varies across the field, because the 11 observations comprising the full *Chandra* exposure have different roll angles.)

Two papers currently in preparation will publish 24 μm fluxes for $\sim$90 X-ray sources in CDF-S (J. Rigby et al. 2004a, 2004b in preparation); most of these sources are within the main sample of this paper.

The Chandra 1 Ms CDF-S is one of the deepest X-ray observations to date. Two reductions and source catalogs exist in the literature. The first is by the CDF-S team, who find 304 sources detected jointly by SExtractor and *wavdetect* (Giacconi et al. 2002, hereafter G02). The second is by the CDF-N team, using the same processing and source extraction methods for CDF-S as they used for CDF-N (Alexander et al. 2003, hereafter A03). Their source catalog has 326 sources. A03 compare these two catalogs, finding 293 sources in common.

Because the *Spitzer* cosmological surveys will also target the CDF-North, in this paper we use the A03 catalog, to facilitate future comparisons between the north and south fields.

The astrometry of the CDF-S *Chandra* catalogs is excellent. A03 registered their astrometry to the frame of the *R*-band ESO Imaging Survey (Arnouts et al. 2001); the median separation between X-ray and *R*-band positions is 0.″37 (A03). Using the

[1] Steward Observatory, University of Arizona, 933 North Cherry Avenue, Tucson, AZ 85721; jrigby@as.arizona.edu.
[2] Osservatorio Astrofisico di Arcetri, INAF, Largo Fermi 5, 50125 Florence, Italy.
[3] Space Science Institute, 4750 Walnut Street, Suite 205, Boulder, CO 80301.
[4] See the catalog at http://www.mpe.de/~mainieri/cdfs_pub.

same *R*-band catalog,[5] we registered our 24 μm mosaic to their astrometric frame by adding a 0.″52 global shift.

The other catalog used in this paper is that of Szokoly et al. (2004, hereafter S04), who present secure spectroscopic redshifts for 137 X-ray–selected sources in the CDF-S. They classify their sources in two ways: based on optical spectra, and based on X-ray luminosity and hardness.

3. SAMPLE SELECTION

We select hard-band (2–8 keV) detections in the CDF-S from the catalog of A03; there are 198. Selecting hard-band detections (rather than soft or any other band detections) reduces contamination from nonactive galaxies. To further maximize the AGN fraction, we require the hard-band flux to exceed 10^{-15} ergs s^{-1} cm^{-2}, which reduces the sample to 157 sources. This is our main sample. None of these sources is classified by S04 as a star or a nonactive galaxy. Almost all of these sources are likely to be AGNs (see Fig. 2 of Barger et al. 2003); 65 have been identified as AGNs by their X-ray hardness and luminosity (which requires a known redshift), and 39 have been identified as AGNs by optical spectroscopy.

Because the soft band of *Chandra* (0.5–2 keV) is more sensitive than the hard band, sources in our main sample generally have a well-measured soft-band flux or a well-constrained limit.

For the main sample, we seek redshifts as available from S04. S04 targeted optical counterparts to X-ray sources from the G02 catalog (and thus associate redshifts with G02 X-ray sources), whereas we use the A03 X-ray catalog. As a result, it is necessary to associate the A03 and S04 catalogs, which we do by matching sources whose coordinates are separated by less than 2″. Such a large separation is necessary to match sources at large off-axis angles, where *Chandra* centroiding is difficult. Since the only spectra in the S04 catalog are counterparts to X-ray sources, the source density is small ($\sim$0.5 arcmin^{-2}), so the probability of false matches with the A03 X-ray catalog is small. In the main sample, 65 AGNs have secure redshifts and optical classifications.

For each X-ray source in our main sample, we search for a 24 μm counterpart from our catalog. To claim detection, we require the fractional flux uncertainty to be below 50% and the coordinates (X-ray and 24 μm) to be offset by less than 1.″2. (This small separation is sufficient to match sources over most of the field and is necessary to prevent false matches, since the 24 μm source density is high.) No X-ray source has multiple 24 μm sources within the permitted offset. Given the 24 μm source density reported above, for the main sample of 157 X-ray sources, by chance we expect $\sim$1 false 24 μm counterpart using the *P* statistic (see, e.g., Lilly et al. 1999). The result of the counterpart search is that 98 of the 157 sources in the main sample have 24 μm counterparts. For sources not detected at 24 μm, we take the flux upper limit to be the 80% completeness limit (0.083 mJy).

Figure 1 (Plate 1) displays the section of the 24 μm mosaic that overlaps the Chandra field, with the main sample X-ray positions overlaid.

4. COMPARING X-RAY AND 24 μm COLORS

AGNs are traditionally classified by optical spectroscopy. However, for distant sources, nuclear emission can be overwhelmed by stellar emission, especially for low-luminosity AGNs (Moran et al. 2002). Obscuration or lack of narrow lines may also play a role (Maiolino et al. 2003). Consequently, 43% of X-ray–selected AGNs in the CDF-S are not classified as active by optical spectroscopy (S04). Because of this, many authors have argued that X-rays are a better way to *select* AGNs than optical spectroscopic surveys.

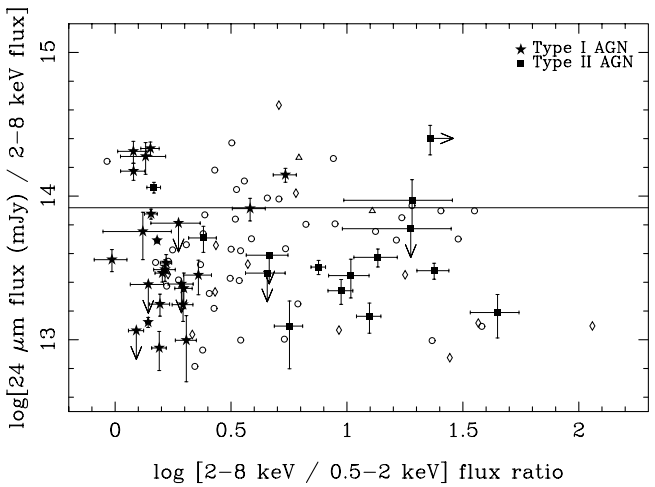

FIG. 2.—Comparison of optical and X-ray AGN classification. Symbol types indicate classification from optical spectroscopy: broad-line AGNs and QSOs (*star symbols*), and AGNs with high-excitation narrow lines (*filled squares*). These are the classical type 1 and type 2 categories, respectively. Also plotted are sources whose optical spectra show low-excitation emission lines (*diamonds*) or absorption lines (*triangles*), as well as sources lacking optical classification (*circles*). To improve plot clarity, for the last three categories, sources with nondetections in 24 μm or soft X-ray are omitted, and error bars are omitted. Optical spectroscopy and classification are from S04.

Furthermore, X-rays can provide a more effective way to *classify* AGNs (Hasinger et al. 2001). AGNs with harder X-ray spectra are generally measured as having thicker columns of absorbing gas than X-ray–soft AGNs. Similarly, in unification models, optical type 2 AGNs are drawn from the same population of objects as type 1 AGNs, but they are viewed through thicker columns of obscuring gas and dust. Thus, X-ray hardness can estimate the obscuration of AGNs when optical spectroscopy cannot.

Figure 2 compares optical and X-ray classification of the CDF-S AGNs. The *x*-axis is an indicator of spectral hardness: we define the ratio of the hard to soft X-ray fluxes as $H/S = \log\left[\text{flux}(2\text{–}8\text{ keV})/\text{flux}(0.5\text{–}2\text{ keV})\right]$. Sources with broad emission lines (optically selected type 1 Seyferts and QSOs) cluster toward the X-ray–soft side of the figure. These objects are well separated in X-ray hardness from the sources with optical high-excitation narrow emission lines (optically selected type 2 AGNs), which span a range of higher X-ray hardness. This clear separation validates the use of the hard/soft X-ray flux ratio *H/S* as a tool to classify AGNs, as also found by Mainieri et al. (2002). Indeed, S04 also used X-ray hardness to classify these CDF-S AGNs using the same *Chandra* data and very similar energy bands to this work, but with a counts ratio rather than a flux ratio; their division between type 1 and type 2 AGNs lies at $H/S \approx 0.6$ in our Figure 2 and agrees well with the boundary between optically classified type 1 and 2 AGNs.

In Figure 3, we examine how X-ray hardness affects the behavior of the 24 μm to X-ray flux ratio, defined as $24/\text{X} = \log\left[(24\,\mu\text{m flux density, mJy})/(2\text{–}8\,\text{keV flux, ergs s}^{-1}\text{cm}^{-2})\right]$. There is a factor of 100 spread in both the *H/S* and 24/X flux

[5] From CDS, at http://vizier.u-strasbg.fr.

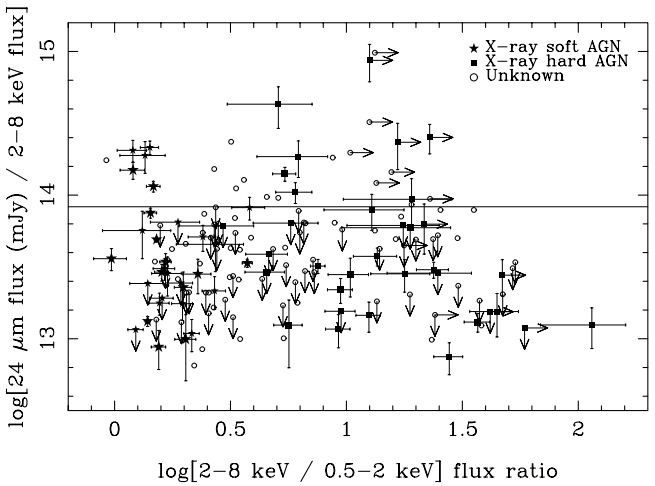

FIG. 3.—IR/X-ray color vs. X-ray hardness. All sources in the main sample are plotted, and symbol types indicate X-ray classification from S04: X-ray–classified soft AGNs (*star symbols*), X-ray–classified hard AGNs (*filled squares*), and unclassified sources (*circles*). Sources lacking measured redshifts are "unclassified," since a redshift is necessary to measure the X-ray luminosity, which S04 required along with X-ray hardness to classify sources. For clarity, error bars are not plotted for the unclassified sources. Larger symbols indicate QSO luminosities.

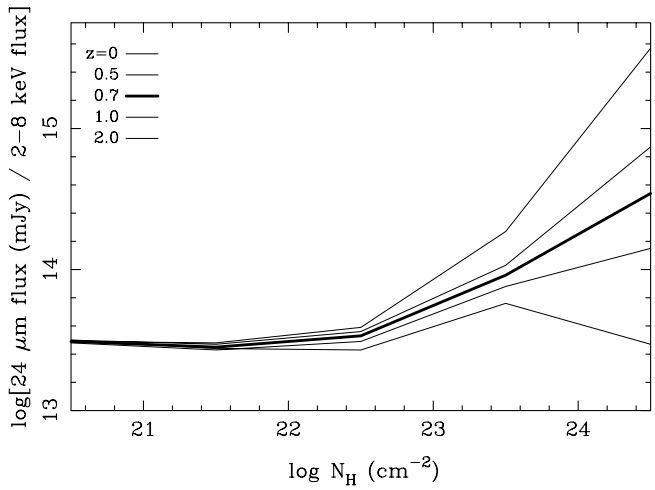

FIG. 4.—Behavior of the 24 μm/2–8 keV flux ratio with increasing obscuration. From top to bottom, lines show line ratios for local templates (Silva et al. 2004), redshifted to $z = 0$, 0.5, 0.7 (*dark line*), 1.0, and 2.0. Intrinsic differences in the template SEDs create a 24/X scatter of about ± 0.5 dex around the mean values plotted.

ratios. The spread in *H/S* reflects the range of X-ray hardness found in AGNs. We discuss the reasons for the spread in the 24/X flux ratio below.

The horizontal line in Figures 2 and 3 is the 24/X color of a source with hard X-ray flux at the sample cutoff and 24 μm flux at the 80% completeness limit. Since the sample is X-ray selected, it is reasonably complete to colors above the line, while it may be missing sources with colors below the line (because the 24 μm flux may fall below the detection limit).

Figures 2 and 3 show that overall, the 24 μm/2–8 keV flux ratio does *not* depend on the hardness of the AGNs. There is no global trend of 24/X with *H/S*. Nor does 24/X ratio differ significantly between the X-ray–classified hard and soft AGNs in Figure 3 or between the optically classified type 1 and type 2 AGNs in Figure 2.

Fadda et al. (2002) found that 5–10 keV *XMM-Newton* sources were twice as likely to have 15 μm counterparts compared with 0.5–2 keV sources; however, this result was based on just 28 IR-detected hard X-ray sources. The authors used the IR/X-ray spectral slope to classify sources as type 1 or type 2 AGNs or dominated by star formation, and then applied these classifications to estimate the AGN contribution to the IR background. (They did find some X-ray–soft AGNs with high IR/X ratios, which they attributed to host galaxy contamination.) As discussed above, our full sample (Fig. 3) contradicts the Fadda et al. (2002) result that the mid-IR flux of AGNs is a strong function of X-ray hardness.

5. DISCUSSION

To understand the behavior of the 24 μm/2–8 keV flux ratio, in Figure 4 we present the flux ratios predicted by local AGN templates with a range of obscuration (Silva et al. 2004). These templates were obtained by interpolating nuclear infrared photometric data of a sample of 33 Seyfert galaxies. Each infrared spectral energy distribution (SED) was normalized to the absorption-corrected hard X-ray luminosity and then averaged within bins of absorbing $N_{\rm H}$. Using these empirical templates, Silva et al. (2004) derived the contribution of AGNs to the mid-IR background and successfully matched the observed fraction.

In Figure 4, at $z = 0$, as the obscuring column increases, the predicted 24/X ratio increases (since the 24 μm flux rises as a result of reprocessing, and the 2–8 keV flux falls dramatically, because of absorption). This effect grows weaker with increasing redshift because of *K*-corrections: as the 2–8 keV band samples progressively higher rest-frame energies, the band is less absorbed for a given column. Generally, in the deep X-ray surveys, type 1 AGNs have $\log N_{\rm H} \lesssim 22$ cm^{-2}, whereas type 2 have $22 \lesssim \log N_{\rm H} \lesssim 24$ cm^{-2} (Gilli 2004).

A basic conclusion from Figure 4 is that local AGNs with $\log N_{\rm H} \lesssim 23.2$ cm^{-2} cannot produce 24/X > 14 for $0 < z < 2$. When X-ray–soft AGNs are observed to have such high 24/X ratios (as seen for a minority of sources in Fig. 3), this suggests that the 24 μm flux is dominated by star formation in the host galaxy, not by accretion. (Some of the harder sources with high 24/X may also be star formation dominated.) Using this rule of thumb, we see that star formation does not dominate most of the sources in Figure 3; their 24/X ratios are consistent with AGN power (see also Alonso-Herrero et al. 2004).

To disentangle the effects of redshift and compare the distant AGNs to local templates, in Figure 5 we plot all hard-band detected AGNs in the redshift range $0.65 < z < 0.75$. This range encompasses the prominent $z = 0.674$ and $z = 0.734$ redshift spikes (S04), which allows us to restrict the redshift range (and thus the spread in *K*-correction) while maximizing the sample size.

We first examine the X-ray–soft AGNs in Figure 5. Their 24/X ratios agree well with the local templates, which predict 24/X ≈ 13.5 for AGNs with $\log N_{\rm H} < 22.5$ cm^{-2} at this redshift. The spread in template SEDs predicts a scatter in the flux ratio of about ± 0.5 in log units, which is consistent with the data.

We now examine the 24/X ratio for the hard ($H/S \gtrsim 0.6$) AGNs. We propose two possible interpretations of the trends in Figure 5:

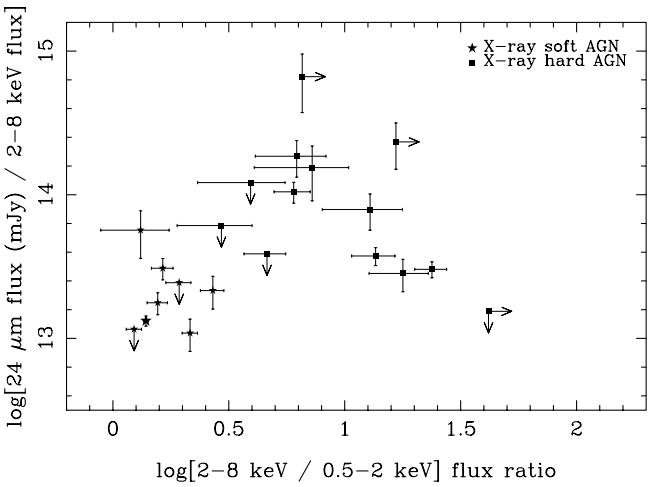

FIG. 5.—IR/X-ray color for the $0.65 < z < 0.75$ AGNs of the CDF-S. All AGNs with spectroscopic redshifts in this range have been plotted; no X-ray flux cut has been imposed. Symbols and classification as in Fig. 3.

1. There is no trend of 24/X with X-ray hardness in Figure 5. The distribution simply reflects the scatter seen in Figure 3.

2. The 24/X ratio does indeed increase with hardness in this subsample, as expected from reprocessing: $H/S \approx 0.8$ AGNs have higher 24/X than the $H/S < 0.5$ AGNs. However, there are several strange exceptions: AGNs with very hard X-ray flux ratios and very low 24/X.

This population of X-ray–hard AGNs with low 24/X is also seen in the full redshift sample (Fig. 3), where there are $\sim$15 such sources. Their 24/X ratios are 0.5–1 dex lower than that predicted by the templates. These sources are surprising within the unification paradigm: the hardness ratios indicate large column density, which unification scenarios associate with a dusty molecular torus; this column should absorb the X-ray radiation, thus increasing 24/X relative to lower column AGNs. Additionally, dust in the torus should absorb a large fraction of the UV continuum and re-emit that energy in the mid-infrared, further increasing 24 μm/X. In the X-ray–hard, 24 μm–faint sources in question, this expectation is not observed. Thus, these sources merit further investigation; there may be a real difference between these AGNs and local AGNs (for example, in their dust properties or absorbing geometries). Although the average 24/X value for the X-ray–hard AGNs may be higher than it appears in Figure 3 because of selection effects, the sources with low 24/X still beg explanation.

While the *H/S* X-ray flux ratio is a useful diagnostic, the more fundamental parameter is the amount of obscuring column. For the very hard ($H/S > 1$) AGNs with known redshifts, we examine the X-ray spectral information derived by Gilli (2004). Ten of the 16 spectra are fitted by $\log N_{\rm H} \approx 23$ cm^{-2}, while only five fits require $23.7 < \log N_{\rm H} < 24$ cm^{-2}. Those five nearly Compton thick AGNs have 24/X values spanning 13.2–14.4, which is the same range populated by the other AGNs (soft and hard).

Could we have missed the majority of the highly obscured, high 24/X AGNs? Since Compton-thick AGNs should be fainter at 2–8 keV than less obscured AGNs, it is quite possible that the most obscured AGNs are the faintest in our survey. The faint (hard flux $\lesssim 3 \times 10^{-15}$ ergs s^{-1} cm^{-2}) AGNs are less likely to have known spectroscopic redshifts and reliable X-ray spectral fits. Since they are faint in the hard band and undetected in the soft, they have lower limits on *H/S* that permit but do not require extreme hardness. Several such objects have high 24/X. Thus, these AGNs are good candidates for being highly obscured. If they are, they would populate the high-*H/S*, high-24/X region of Figure 3 where obscured AGNs are expected but not seen.

6. CONCLUSIONS

We present the first look at the 24 μm to X-ray colors of X-ray–selected AGNs. The expectation that harder AGNs should be relatively brighter at 24 μm is not confirmed. Rather, there is large scatter and no trend in 24 μm/2–8 keV color with X-ray hardness in our sample of 157 AGNs (with dynamic range of 100 in both flux ratios). In addition, the 24/X colors of optically identified type 1 and 2 AGNs are indistinguishable.

In a narrow redshift slice (picked to minimize differential *K*-corrections), we see hints that 24/X may increase with X-ray hardness (though this effect is not seen in the full sample). However, in both the restricted-redshift and full samples, we identify AGNs with unusual colors: very hard X-ray flux ratios and surprisingly low 24/X ratios. These AGNs merit further investigation.

X-ray spectral fits to 16 of the X-ray–hard AGNs find column densities of 10^{23}–10^{24} cm^{-2}, most toward the lower end of this range. Thus, only a handful are nearly Compton-thick ($N_{\rm H} \approx 10^{24}$ cm^{-2}). Even these sources do not distinguish themselves in 24/X color from the lower column AGNs.

Thus, while this initial survey has not yet confirmed expectations for a population of X-ray–obscured, infrared-bright AGNs, we have raised new questions: What explains the factor of $\sim$100 range in 24 μm to 2–8 keV flux ratio? Why do many of the hardest AGNs have very low 24/X ratios compared with local templates? And if hard X-ray selection and 24 μm follow-up finds few Compton-thick AGNs, what is a better way to search? Future surveys and follow-up observations are clearly needed to address these questions.

We thank all who made *Spitzer* a reality. We also thank the CDF-North team for making available *Chandra* fits images of the CDF-South. This work is based in part on observations made with *Spitzer*, which is operated by the Jet Propulsion Laboratory, California Institute of Technology, under NASA contract 1407. Support for this work was provided by NASA through contract number 960785, issued by JPL/Caltech.

REFERENCES

Alexander, D. M., et al. 2003, AJ, 126, 539 (A03)
Alonso-Herrero, A., et al. 2004, ApJS, 154, 55
Arnouts, S., et al. 2001, A&A, 379, 740
Barger, A. J., et al. 2003, AJ, 126, 632
Comastri, A., Setti, G., Zamorani, G., & Hasinger, G. 1995, A&A, 296, 1
Dole, H., et al. 2004, ApJS, 154, 93
Fadda, D., Flores, H., Hasinger, G., Franceschini, A., Altieri, B., Cesarsky, C. J., Elbaz, D., & Ferrando, P. 2002, A&A, 383, 838
Franceschini, A., Fadda, D., Cesarsky, C. J., Elbaz, D., Flores, H., & Granato, G. L. 2002, ApJ, 568, 470
Giacconi, R., et al. 2002, ApJS, 139, 369 (G02)
Gilli, R. 2004, Adv. Space Res., in press (astro-ph/0303115)

Gilli, R., Salvati, M., & Hasinger, G. 2001, A&A, 366, 407
Gordon, K. D., et al. 2004, PASP, submitted
Hasinger, G., et al. 2001, A&A, 365, L45
Lilly, S. J., et al. 1999, ApJ, 518, 641
Madau, P., Ghisellini, G., & Fabian, A. C. 1994, MNRAS, 267, L17
Mainieri, V., Bergeron, J., Hasinger, G., Lehmann, I., Rosati, P., Schmidt, M., Szokoly, G., & Della Ceca, R. 2002, A&A, 393, 425
Maiolino, R., et al. 2003, MNRAS, 344, L59
Moran, E. C., Filippenko, A. V., & Chornock, R. 2002, ApJ, 579, 71
Papovich, C., et al. 2004, ApJS, 154, 70
Rieke, G. H., et al. 2004, ApJS, 154, 25
Silva, L., Maiolino, R., & Granato, G. L. 2004, MNRAS, submitted (astro-ph/0403381)
Szokoly, G. P., et al. 2004, ApJS, submitted (astro-ph/0312324)

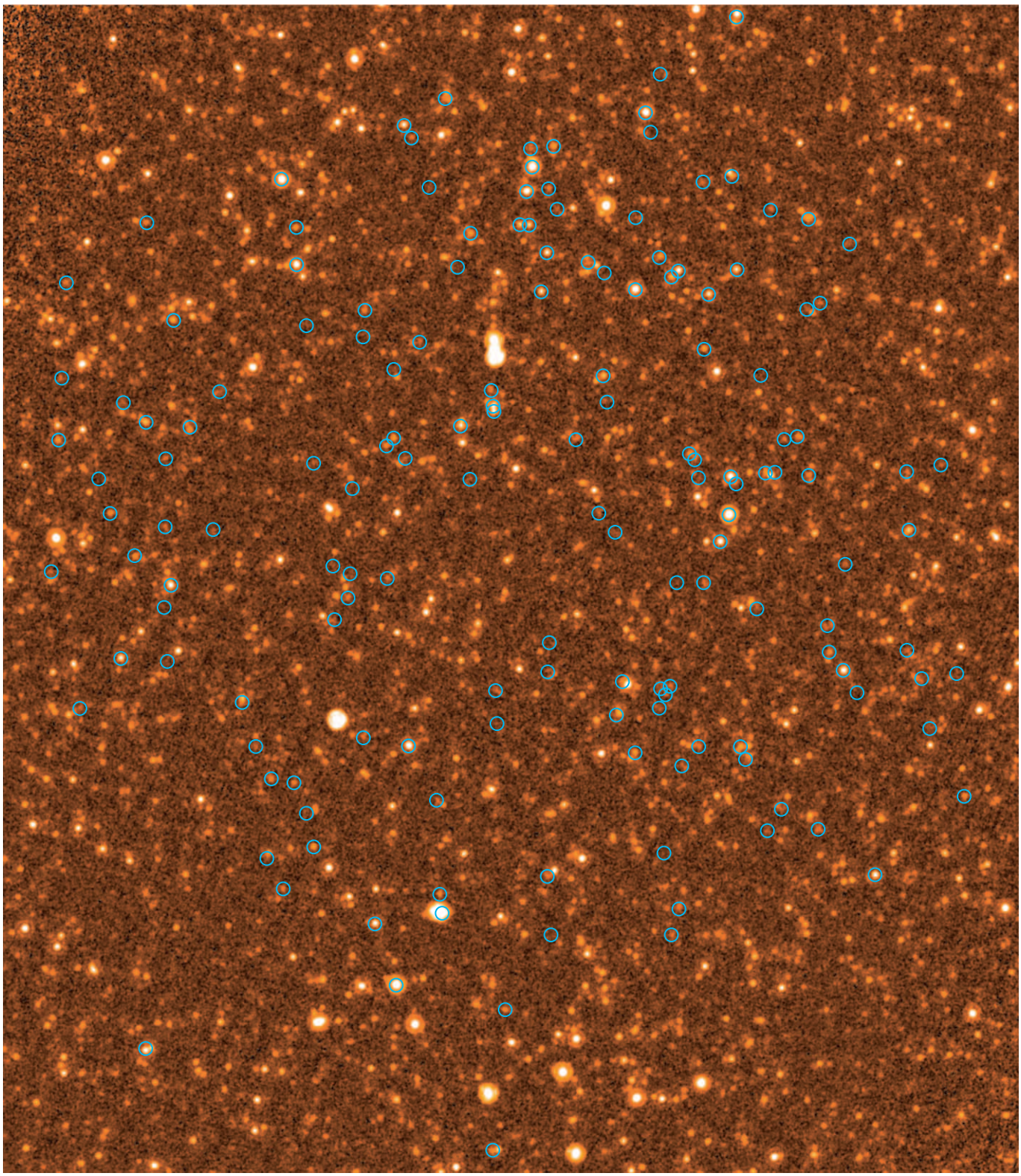

FIG. 1.—CDF-S image at 24 μm. Overplotted are the X-ray positions of the main sample. The circles are large ($R = 8''$) for presentation purposes. The scale is $20.'3 \times 23.'3$; north is up and east is left.

PLATE 1